Modeling low order aberrations in laser guide star adaptive optics systems – KAON 426

Version: 2.3   Date: 21 November 2006

Richard Clare, Marcos van Dam, and Antonin Bouchez

W. M Keck Observatory
California Association for Research in Astronomy
65-1120 Mamalahoa Highway
Kamuela, Hawaii 96743
808-885-7887

Updated 11/21/2006 at 2:00 PM

Abstract

Quasi-static aberrations are observed when using laser guide star (LGS) adaptive optics (AO) systems. These aberrations arise due to the asymmetric elongation of the LGS spots of the Shack-Hartmann wavefront sensor (WFS), quad-cell centroiding, and truncation of the asymmetric LGS spots by the finite extent of the WFS field of view. These LGS aberrations, which can be as much as 1200nm RMS, vary significantly between nights, due to the difference in sodium structure between nights. In this report, we successfully model these LGS aberrations for the Keck II LGS AO system. We use this model to characterize the LGS aberrations as a function of pupil angle, elevation, sodium structure, uplink tip/tilt error, field stop geometry, detector field of view, the number of detector pixels, and seeing. We also employ the model to estimate the LGS aberrations for the Palomar AO system, the future Keck I LGS AO and Keck II LGS AO systems, and the TMT LGS AO system. The LGS aberrations are significantly reduced by projecting the laser from behind the secondary compared to side projection.

Table of Contents
(NB: Please note that section numbers will change as the document evolves).

1   Introduction

Laser guide star (LGS) aberrations show up as the difference between the natural guide star (NGS) wavefront sensor (WFS) measurements on the low bandwidth WFS (LBWFS) and the time-averaged LGS WFS measurements. The purpose of this report is to model the LGS aberrations observed at WM Keck Observatory and compare with the measured aberrations, to understand the effect of individual parameters on the LGS aberrations, and to then use the model to extrapolate to future systems.

The Keck II AO system has a Shack-Hartmann WFS. For a Shack-Hartmann sensor with a LGS at a finite height, the spot at each subaperture is elongated due to the parallax effect. The elongation of the Shack-Hartmann spots, η, for the LGS WFS is approximately given by [1]

$$\eta \approx \frac{\cos(\zeta)bt}{h^2} \qquad (1)$$

where ζ is the zenith angle, b is the baseline distance between the launch telescope and the subaperture, t is the thickness of the sodium layer, and h is the height of the sodium layer above the telescope.

The exact expression for the elongation of a Shack-Hartmann LGS spot is given by considering Fig. 1. The elongation is the difference between the angle from which the subaperture sees the top of the sodium layer, β, and the angle from which the subaperture sees the bottom of the sodium layer, α.
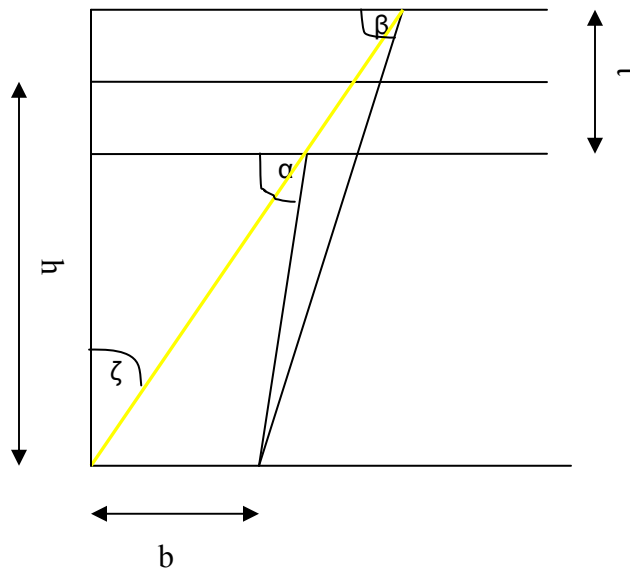
Figure 1 – Geometry of the LGS problem. The subaperture is at a baseline b from the laser, which is launched at a zenith angle ζ. The sodium layer of thickness t is at an altitude h. The subaperture sees the bottom of the sodium layer at an angle α, and the top of the sodium layer at an angle β.

The exact form of the elongation is then:

$$\eta = \beta - \alpha$$

$$\eta = \tan^{-1}\left(\frac{h+t/2}{b+(h-t/2)/\tan(\pi/2-\zeta)}\right) - \tan^{-1}\left(\frac{h+t/2}{b+(h+t/2)/\tan(\pi/2-\zeta)}\right) \tag{2}$$

The sources of the LGS aberrations are identified in Ref. [1], and are summarized here:
1. Asymmetric spot elongation: the LGS spots are asymmetric because the elongation is inversely proportional to height squared (see Eq. (1)), so the bottom of the profile appears more elongated than the top of the profile.
2. Quad-cell centroiding: for an asymmetric LGS spot, the quad-cell centroid is not equal to the center-of-mass of the LGS spot.
3. Truncation of the LGS spots: a bias is introduced to the centroid measurement if the LGS spot is asymmetric and truncated.
4. Telescope and AO system aberrations: because the laser guide star is situated at ~90km and the NGS at infinity, the LGS and NGS focal planes are different.

The LGS aberrations are calculated as a least squares fit to the low order Zernike terms from the displacements (centroids) of each subaperture. We choose to use Zernikes to model the aberrations because the low order terms represent the well known optical aberrations of astigmatism, coma etc. The first 10 Zernikes (i.e. up to spherical aberration, but ignoring tip, tilt and focus which are independently corrected) contain 89% of the mean-squared LGS aberrations. That is 89% of the mean-squared aberrations as seen on the DM (Figure 2) can be fitted with these seven Zernike terms.
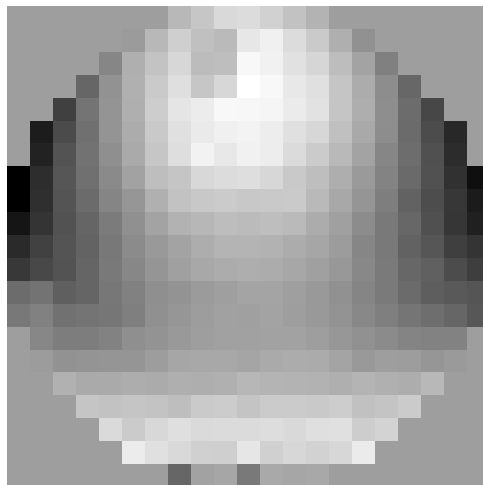

Figure 2 – The phase on the DM representing the LGS aberrations for a pupil angle of 0 degrees for Keck II.

The LGS aberrations are measured on the telescope by locking the tip/tilt loop on a bright NGS, and by locking the deformable mirror loop on the LGS and setting the LGS reference centroids to be all zeros. The pupil is kept fixed on both the LGS WFS and LBWFS. The pupil angle was rotated and LBWFS images taken at regular intervals. The laser is located at the top of the pupil for Keck II when the pupil angle is 116.6 degrees. We will define a pupil angle of 0 degrees to be at the top of the pupil in this report in order to be consistent between telescopes. Thus the pupil angles reported here for Keck lead the Keck pupil angle by 116.6 degrees.

We display the measured LGS aberrations versus pupil angle for the astigmatism, coma, and spherical aberrations, as well as the total low order LGS aberrations for the nights of 26 January 2005 and 20 July 2006 in Fig.'s 3-8. These observations were made near zenith. A best-fit spline is superimposed for each mode. We see from these graphs that there are significant astigmatism, coma and spherical LGS aberrations and that these aberrations vary with pupil angle. More specifically, we note that:

1. The astigmatism modes both exhibit sinusoidal behavior with π periodicity with respect to pupil angle. The astigmatism modes are non-zero mean on both nights. The peaks and valleys of both astigmatism modes are different on the two cycles. This is consistent between the two nights.
2. The coma modes also exhibit sinusoidal behavior with respect to pupil angle, with 2π periodicity. Both the coma modes are non-zero mean on both nights.
3. The spherical aberration is non-zero mean on both nights. Any dependence of the spherical aberration on the pupil angle is not clear from these nights.
4. There is significant variation in the magnitudes of LGS aberrations between the two nights, although the phase of the astigmatism and coma modes is consistent between nights. The spherical aberration is particularly inconsistent between nights, with the mean differing by approximately a factor of seven.
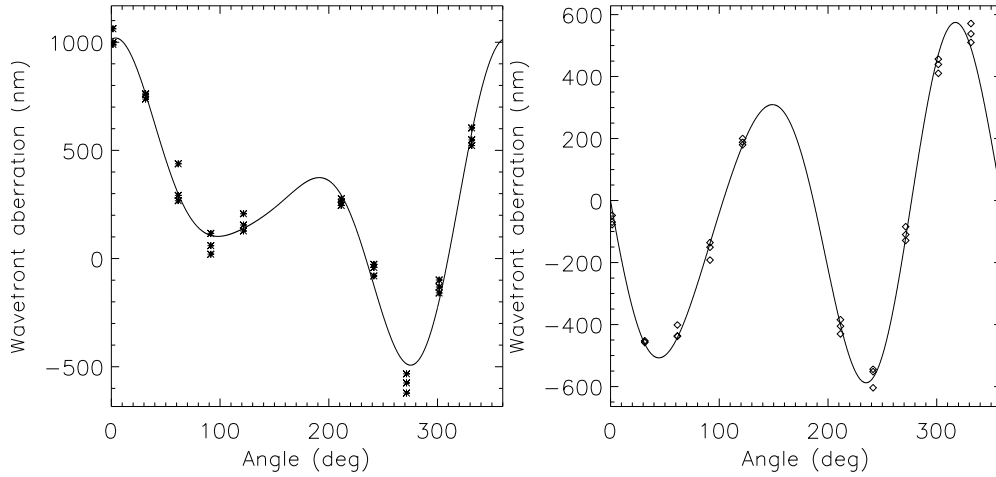
Figure 3 - The measured magnitude of the 0 degree astigmatism (left) and 45 degree astigmatism LGS aberration modes (right) for the night of 26 January 2005.
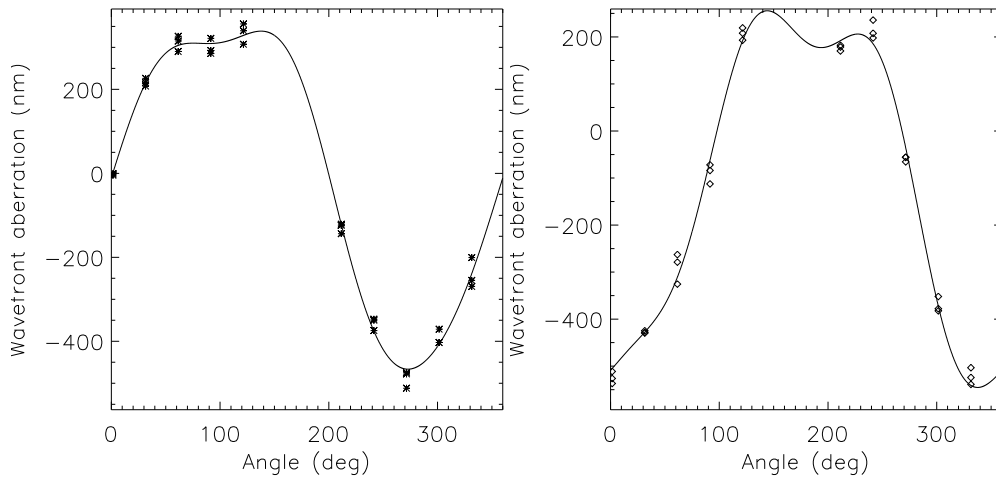

Figure 4 - The measured magnitude of the y coma (left) and x coma (right) LGS aberration modes for the night of 26 January 2005.
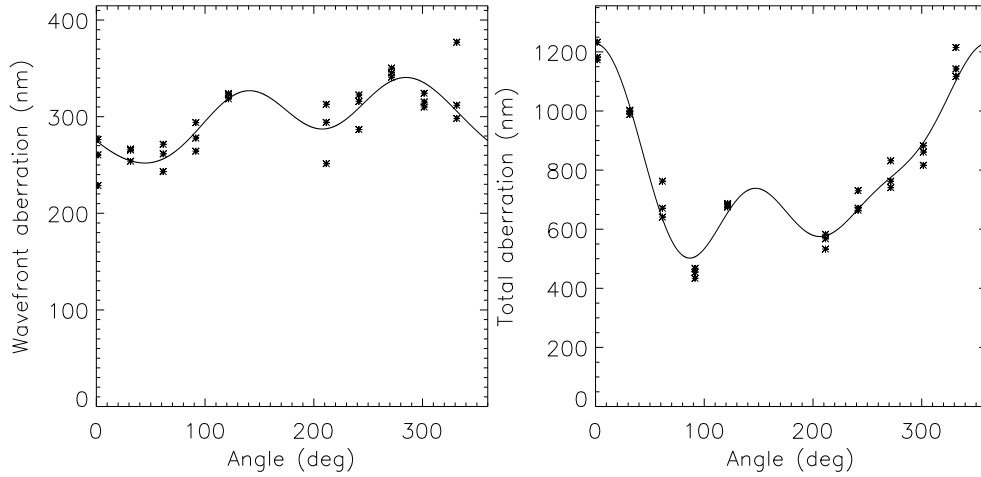
Figure 5 - Left: The magnitude of the measured spherical LGS aberration for the night of 26 January 2005. Right: The total magnitude of the low order LGS aberration for the night of 26 January 2005.
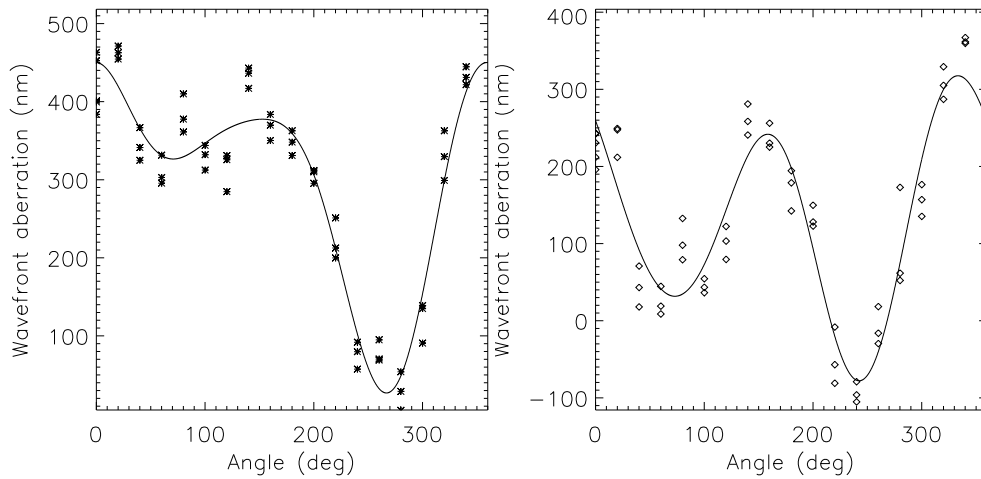

Figure 6 - The magnitude of the measured 0 degree astigmatism (left) and 45 degree astigmatism LGS aberration modes (right) for the night of 20 July 2006.
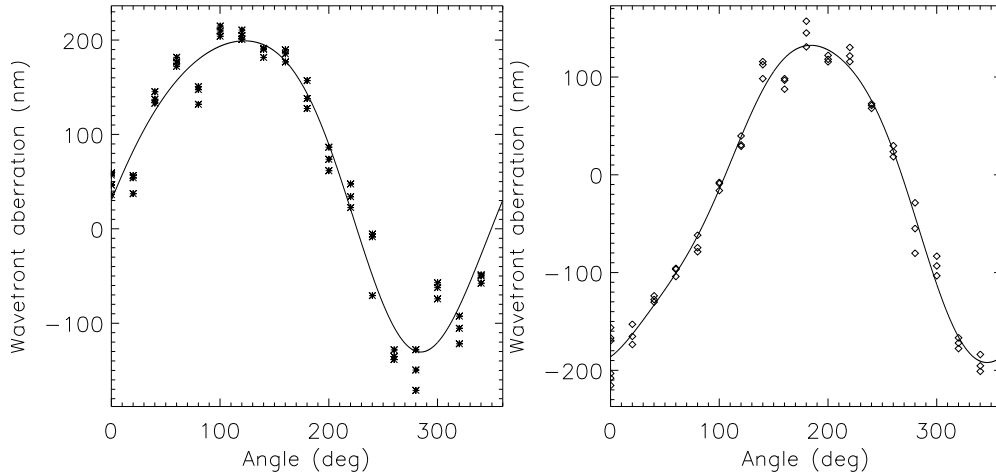
Figure 7 – The magnitude of the measured y coma (left) and x coma (right) LGS aberration modes for the night of 20 July 2006.
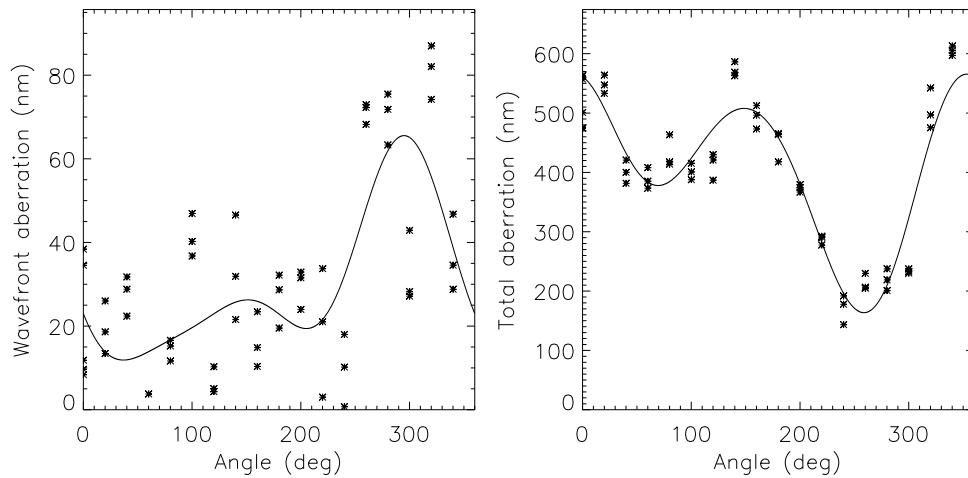
Figure 8 – Left: The magnitude of the measured spherical LGS aberration for the night of 20 July 2006. Right: The total magnitude of the low order LGS aberration for the night of 20 July 2006.

The LGS aberrations are also a function of the zenith angle, and the dependence is shown for the astigmatism and coma modes in Fig. 9 for the night of 7 October 2004. For all of these modes, the magnitude of the LGS aberrations increases with increasing elevation.
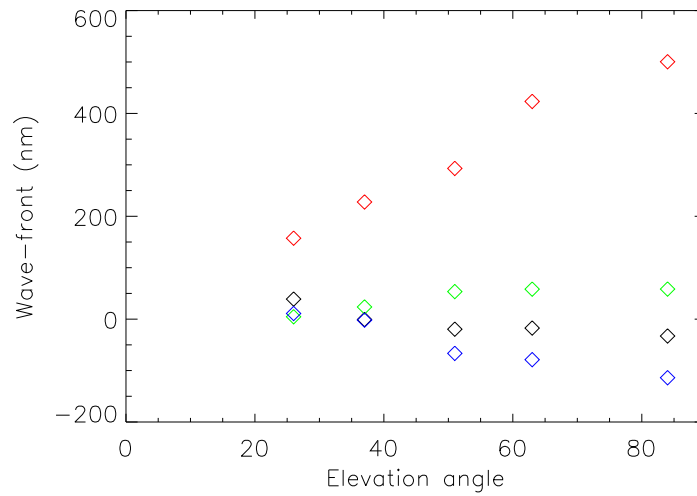
Figure 9 – The measured aberrations as a function of elevation angle (90-zenith angle) for the night of 3 October 2004 for a zero degree pupil angle. The curves are 0 degree astigmatism (black), 45 degree astigmatism (red), y coma (green), and x coma (blue).

The previous figures displayed the LGS aberrations in open loop, i.e. the reference centroids were set to all zeros and the LGS aberrations calculated from the LGS WFS centroids on dedicated engineering runs. We have also monitored the residual LGS aberrations while astronomical observations are carried out in closed loop, i.e. the LGS WFS reference centroids are updated so as to cancel the LGS aberrations. In Figure 9, we plot the LGS aberrations recorded over several LGS nights for the month of June 2006 on Keck II. In closed loop, the LGS aberrations are calculated with a least-squares fit of the low order Zernike modes to the reference centroids for the LGS WFS. Clearly the LGS aberrations are not consistent from night to night.
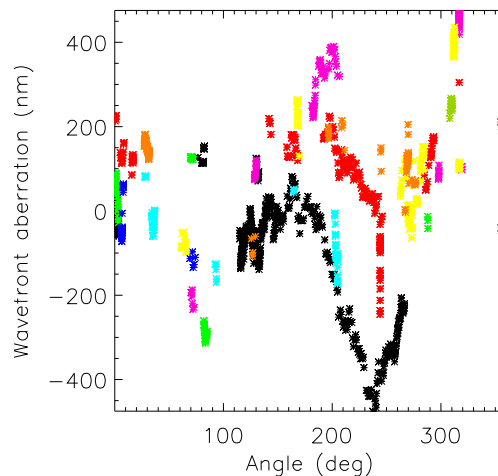

Figure 10 – The LGS aberrations (0 degree astigmatism) versus pupil angle when operating in closed-loop. The data was collected over June 2006, and has been thresholded to zenith angles less than 35 degrees and convergence of the LGS aberration to less than 150nm. The different colored data points represent different nights.

The format for the rest of this document is as follows: in Section 2 we model the Keck II LGS aberrations and compare with the observed LGS aberrations. In Section 3, we investigate the parameter space that affects the LGS aberrations. In Section 4, we estimate the LGS aberrations for planned future AO systems. Finally, in Section 5, we draw our conclusions on the LGS aberrations.

2   Modeling the Keck II system

In this section, we model the Keck II LGS aberrations as a function of pupil angle and compare with the measured aberrations. The Keck II LGS AO system has a 589 nm wavelength laser which is propagated 6.2m from the optical axis of the telescope. The Keck II LGS wavefront sensor is a Shack-Hartmann sensor, consisting of 304 subapertures, although the reconstruction at any one time is made from the brightest 240 subapertures. The detector for each subaperture is a quad-cell, with each pixel 2.1'' square. There is a circular field stop of radius 2.4'' located at the focus of the telescope.

The LGS spots are calculated by ray tracing a cylinder for each pixel in the detector through the atmosphere and integrating the sodium profile within the illuminated cylinder. The diameter of the illuminated cylinder is assumed to be 50cm. First, the LGS images are calculated for well-sampled spots, as shown in Fig. 11 for all the 304 subapertures for Keck II. These well-sampled images are then binned to form the quad-cell images, displayed in Fig. 12. For the images shown in Fig. 11, the minimum FWHM is 1.66'', and the maximum FWHM is 4.63'', which means that the most elongated spots are significantly larger than the detector FOV of 4.2''.
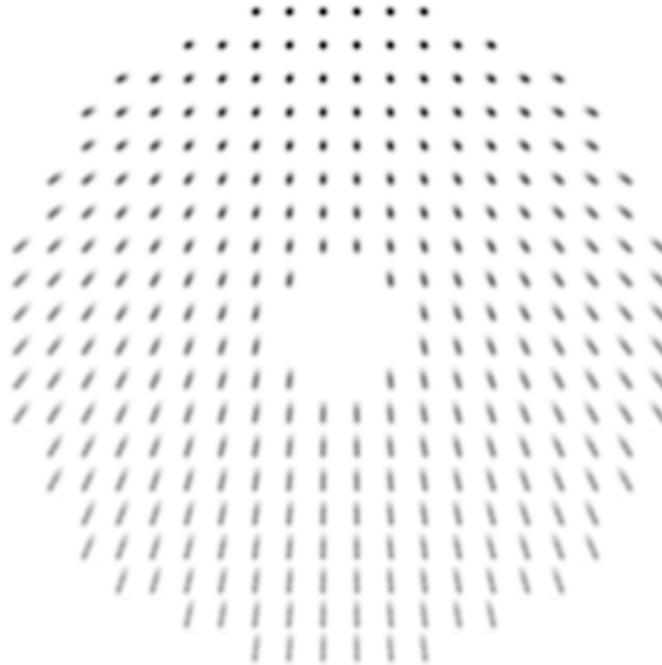
Figure 11 – The simulated well-sampled images for Keck II LGS Shack-Hartmann WFS. The laser is at the top of the pupil for a pupil angle of 0 degrees.
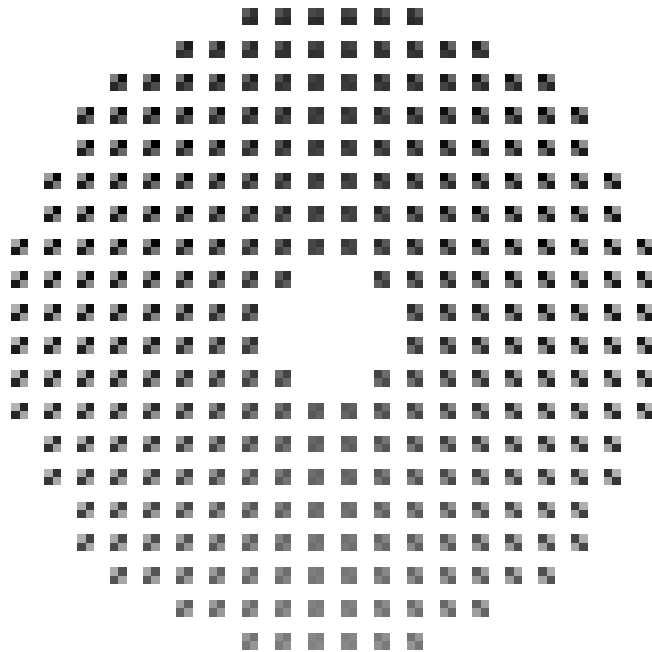

Figure 12 – The simulated quad-cell images for the Keck II LGS Shack-Hartmann WFS. The laser is at the top of the pupil.

The LGS aberrations are calculated as a least squares fit to the low order Zernike terms from the displacements of each subaperture. The LGS images have uplink tip/tilt correction such that the mean centroid of all the subaperture images is zero in both x and y.

The displacement of each subaperture is then calculated as the shift of the subaperture image required to zero the centroid from its zero mean subaperture position.
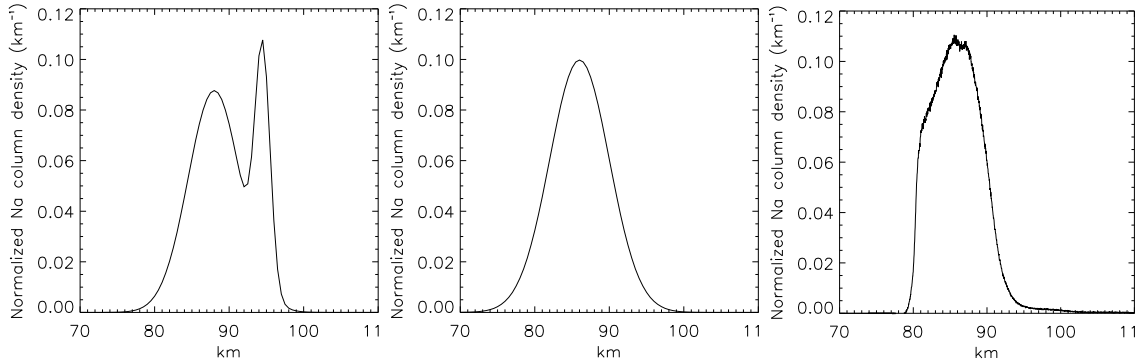

Figure 13 – Left: The normalized sodium profile used in the simulation of the Keck II LGS WFS aberrations. Center: A normalized Gaussian sodium profile. Right: a "median" sodium profile measured with the Colorado state Lidar.

In order to model the Keck II system, we use the sodium profile shown in Fig. 10 (left), which was generated as a best fit of two Gaussians to an acquisition camera image of January 26 2005, shown in Fig. 14.

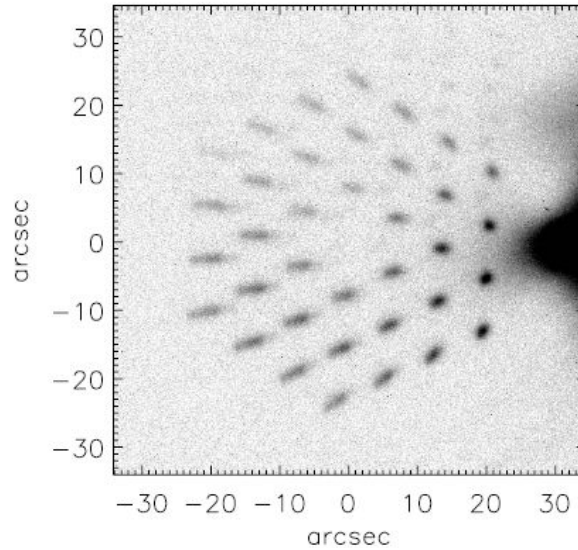**Figure 14 – Acquisition camera (acam) images of the LGS for the night of January 26 2005. The laser is projected from the right-center of the pupil.**

We also use a typical seeing value of 0.5 arc sec. For now, we assume the LGS images are correctly centered on the quad-cells, i.e. there is no uplink tip/tilt error. The modeled LGS aberrations for Keck II at zenith are displayed in Fig.'s 15 and 16.
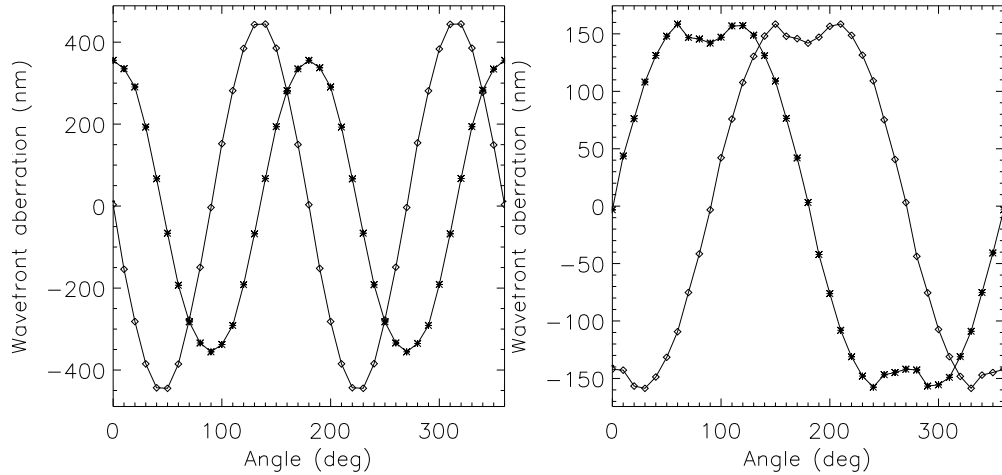
Figure 15 – The simulated magnitude of the LGS aberrations as a function of pupil angle at zenith for Keck II. Left: 0 degree astigmatism (*) and 45 degree astigmatism (◊); Right: y coma (*) and x coma(◊).
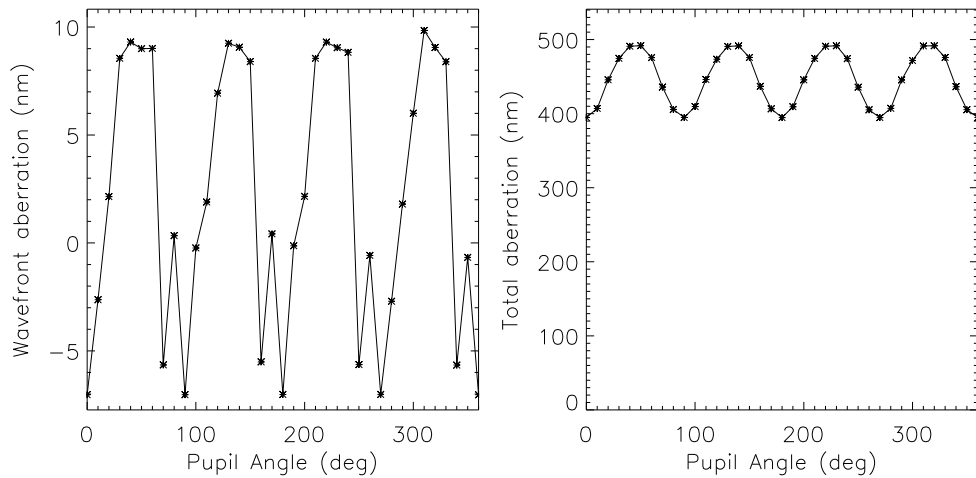

Figure 16 – The simulated magnitude of the LGS aberrations as a function of pupil angle at zenith for Keck II. Left: spherical aberration; Right: The total low order LGS aberrations.

The modeled LGS aberrations exhibit many of the characteristics of the measured LGS aberrations. For both the measured and modeled aberrations, both the astigmatism versus pupil angle curves are approximately sinusoidal and have π periodicity with respect to pupil angle. The modeled and measured astigmatism curves are in phase with each other. The magnitudes of the measured and modeled aberrations agree reasonably, given the imprecise knowledge of the sodium profile and the sodium profile's importance on the magnitude of the LGS aberrations (see section 3.2). The modeled astigmatism curves are zero-mean and the magnitudes of the peaks and troughs are equal in both cycles, unlike the measured aberrations. This thought to be due to an uplink tip/tilt error due to a de-centered field stop, and is investigated in Section 3.3.

The modeled and measured coma versus pupil angle curves are both approximately sinusoidal with the peaks clipped, and 2π periodicity with respect to pupil angle. The modeled and measured coma curves also have the same phase as each other. Unlike the modeled coma curves, the measured coma curves are both non-zero mean, but this can be explained by a UTT error as explained in Section 3.3.

The modeled and measured spherical aberration curves do not agree in either magnitude or phase. The modeled spherical aberration is non-zero mean, and is $\pi/2$ periodic with respect to pupil angle. As will be discussed in Section 3.3, the non-zero mean nature of the measured spherical aberrations cannot be explained by an UTT error. The difference between the measured and modeled spherical LGS aberration could be due to telescope and AO system aberrations which are not modeled here.

The phase aberration represented by the sum of the low order LGS aberrations rotates with pupil angle as shown in Fig. 17. Comparing the total aberration at the 4 different angles shown in Fig. 17 with the astigmatism and coma modes, it is clear that astigmatism is π periodic and coma 2π periodic.
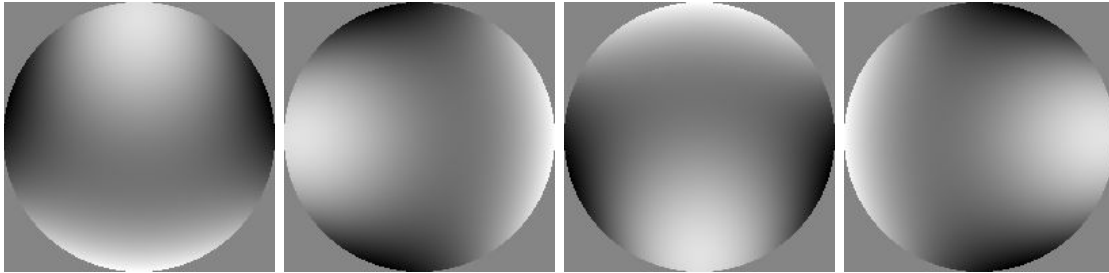

Figure 17 – The total low order phase aberration from left-to-right at 0 degree pupil angle, 90 degrees, 180 degrees and 270 degrees.

3 Parameters

The LGS aberrations are dependent on a number of parameters, and in this section we isolate each of the pertinent parameters, and see how the LGS aberrations are affected for the Keck II system.

3.1 Zenith angle

As shown in Eq. [1], the elongation of the LGS spot is proportional to the cosine of the zenith angle. The seeing also increases by a factor of the secant of the zenith angle to the 3/5ths, although as shown in Section 3.7, the dependence on the seeing is negligible. In Fig. 18, the simulated total low order LGS aberration is plotted versus the zenith angle for a zero degree pupil angle. The total aberration exhibits an approximately cosine dependence on the zenith angle, which is consistent with the LGS elongation being proportional to the cosine of the zenith angle.
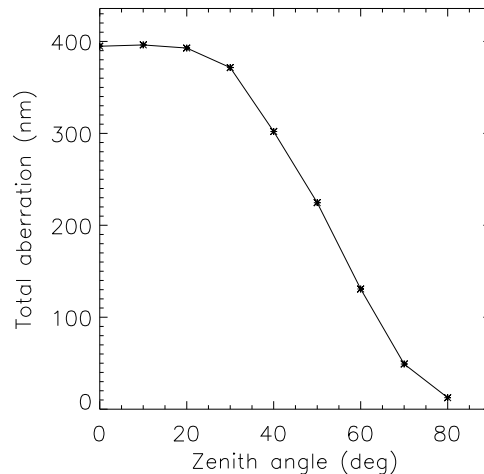
Figure 18 – The total LGS aberration as a function of zenith angle (deg) for the KII system at 0 degree pupil angle.

This result is consistent with the aberrations measured on the telescope and displayed in Fig. 7.

3.2 Sodium structure

The magnitude of the LGS aberrations are strongly dependent on the structure of the sodium layer. The sodium structure can affect the bias due to truncation, and the bias due to using a quad-cell is affected by the asymmetry of the sodium structure. In order to demonstrate and quantify this dependence, we have simulated the Keck II system with the same parameters as Section 2, but using a sodium profile that is a Gaussian with a sigma of 4km, located at an altitude of 86km above the telescope, as shown in Fig. 13 center.

The LGS aberrations for the single Gaussian sodium profile, which are plotted in Fig. 19, are at least four times smaller than for the aberrations for the sum of two Gaussians sodium profile, plotted in Section 2. The spherical aberration for the single Gaussian profile is negligible. For the single Gaussian profile, the 0 degree and 45 astigmatism terms have approximately the same peak values, unlike for the sum of two Gaussians sodium profile. Consequently, the total aberration for the single Gaussian sodium profile is approximately constant with pupil angle.
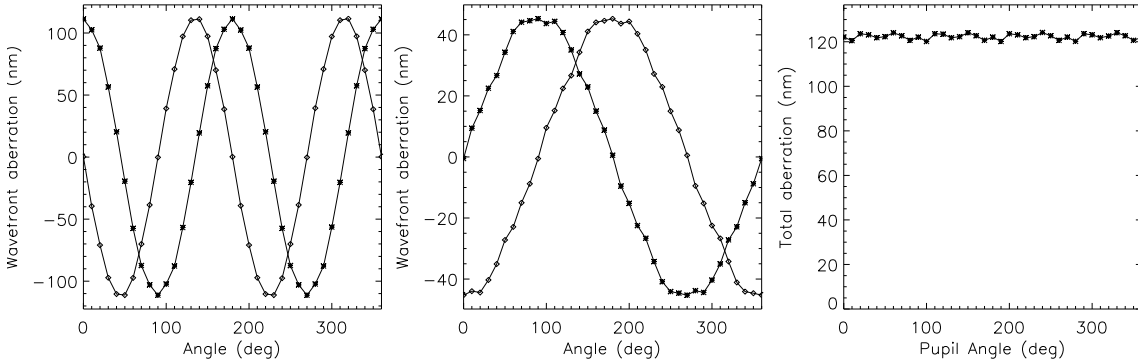
Figure 19 - The simulated magnitude of the LGS aberrations as a function of pupil angle at zenith for a Gaussian sodium profile. Left: 0 degree astigmatism (*) and 45 degree astigmatism (◊); Center: y coma (*) and x coma (◊); Right: the total low order LGS aberration.

We also simulate the Keck II system with the "median" profile as measured by LIDAR at Colorado State University. This profile is shown in Fig 13 (right), and has a vertical resolution of 24m. The LGS aberrations for this measured profile are significantly smaller than the measured LGS aberrations, and the modeled LGS aberrations with either the Gaussian or sum of two Gaussians profiles. This is because the measured profile is narrower than either of the Gaussian profiles, and thus there is less truncation of the LGS spots, which is a significant source of the LGS aberrations. It is also interesting to note that the sign of the astigmatism terms is reversed for this "median" profile compared to the measured LGS aberrations and the modeled aberrations for the Gaussian profiles. This is consistent with Fig. 10, the compilation of closed-loop data over several nights, which shows variation in sign of the LGS aberrations for different nights.
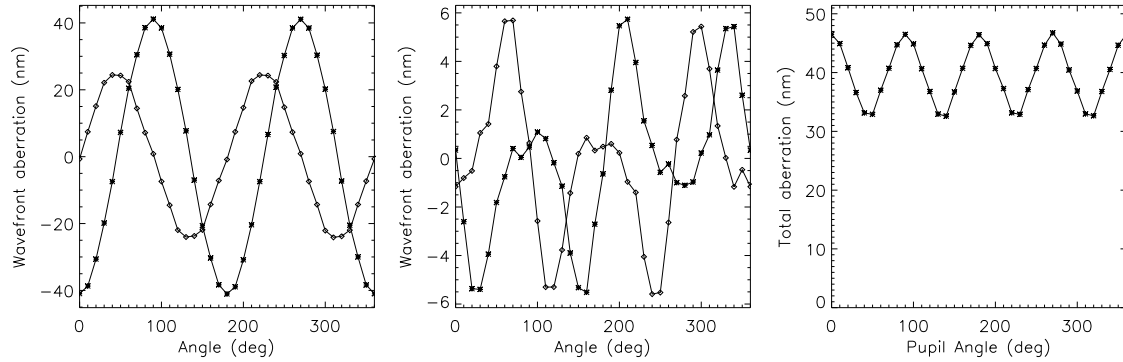
Figure 20 - The simulated magnitude of the LGS aberrations as a function of pupil angle at zenith for the median measured LIDAR profile. Left: 0 degree astigmatism (*) and 45 degree astigmatism (◊); Center: y coma (*) and x coma (◊); Right: the total low order LGS aberration.

3.3   Uplink tip/tilt error

An uplink tip/tilt (UTT) error of the laser beam leads to the LGS subaperture images being de-centered with respect to the subaperture optical axis. This is equivalent to the field stop being de-centered.

For the graphs displayed in this subsection, the subaperture displacements used to calculate the low order Zernike terms are the centroids of each subaperture when the mean centroid of the well-sampled images is set to the uplink tip/tilt error in x and y. This is different to the standard case, where the displacements are calculated as the shift required to zero the centroid of each individual subaperture from the zero mean position.

The astigmatism modes for the nine combinations of positive/negative/zero uplink tip/tilt errors in the x and y directions are plotted in Fig. 21. The coma modes for the same combinations of UTT errors in x and y are plotted in Fig. 22.
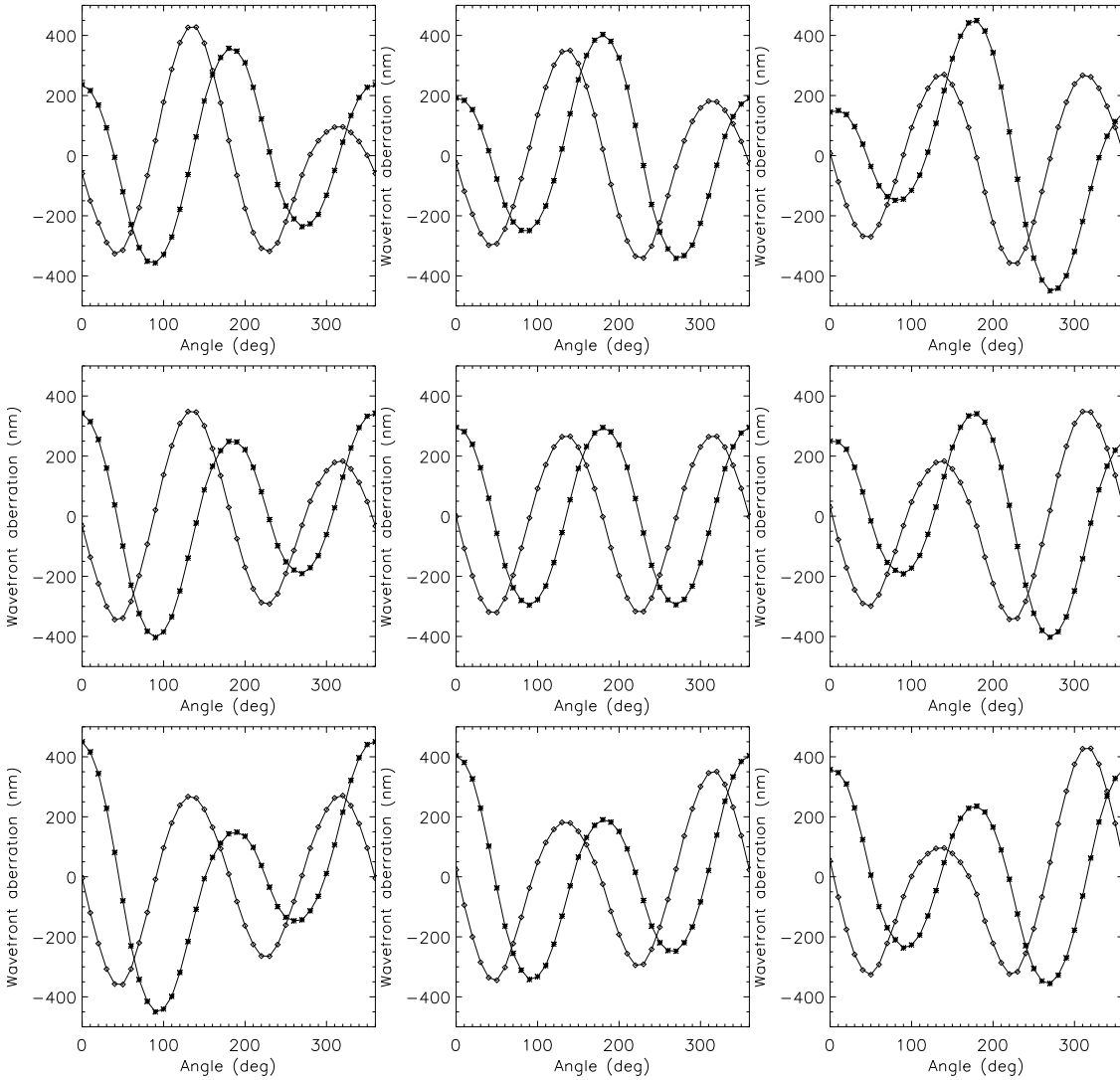
Figure 21 - The simulated magnitude of the LGS astigmatism modes as a function of pupil angle at zenith (* is 0 degree astigmatism and ◊ is 45 degree astigmatism). The uplink tip/tilt error (x,y) in arc sec is from left to right for the top row (-0.1,0.1), (0,0.1), and (0.1,0.1). For the middle row, the UTT error from left to right is (-0.l,0), (0,0) and (0.1,0). For the bottom row, the UTT error is (-0.1,-0.1), (0,-0.1) and (0.1,-0.1).

Figure 22 - The simulated magnitude of the LGS coma modes as a function of pupil angle at zenith (* is y coma and ◊ is x coma). The uplink tip/tilt error (x,y) in arc sec is from left to right for the top row (-0.1,0.1), (0,0.1), and (0.1,0.1). For the middle row, the UTT error from left to right is (-0.l,0), (0,0) and (0.1,0). For the bottom row, the UTT error is (-0.1,-0.1), (0,-0.1) and (0.1,-0.1).
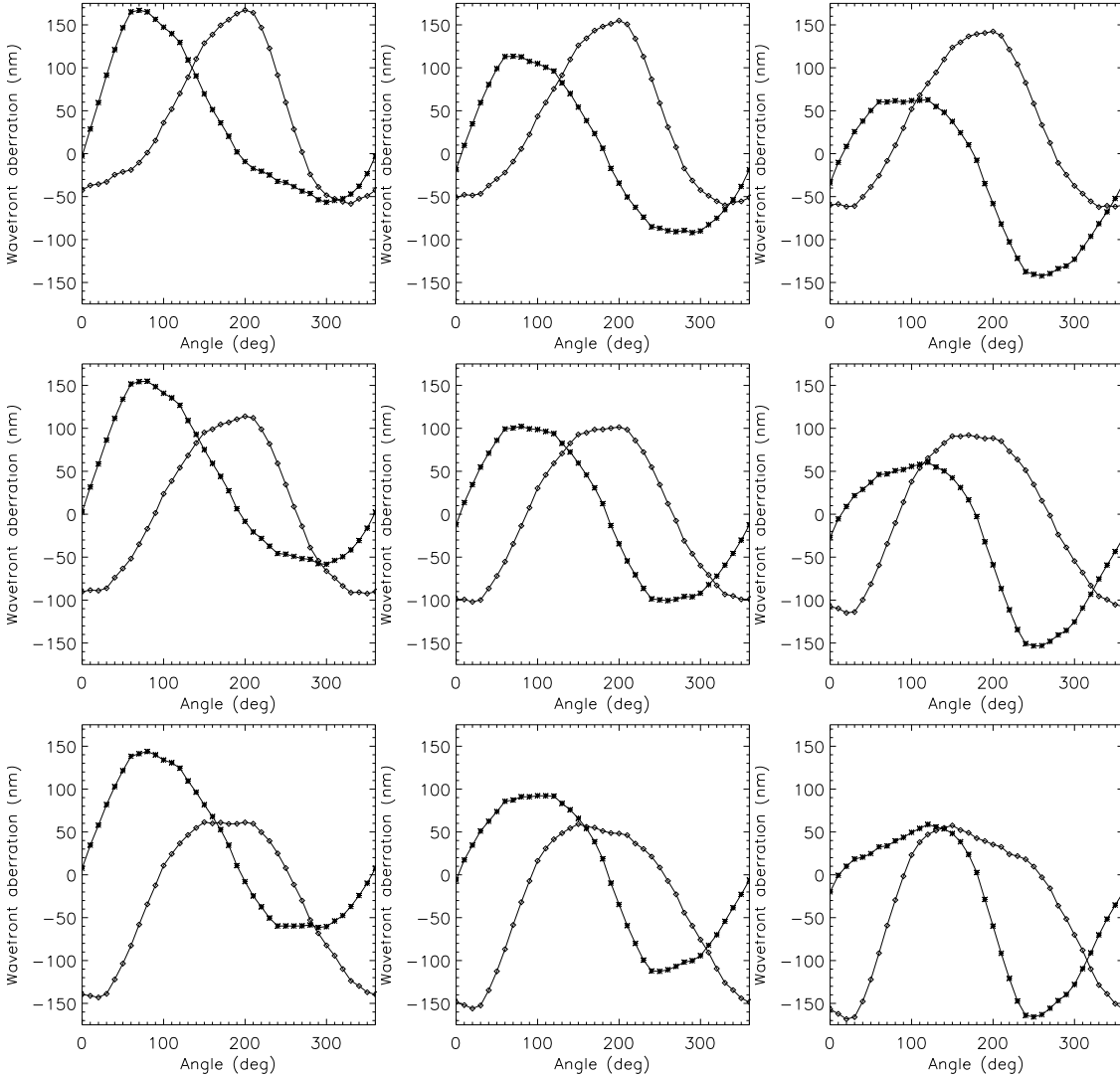
Analysis of Fig.'s 21 and 22 show that the magnitudes of the peaks and nulls of the approximately sinusoidal astigmatism and coma curves as a function of pupil angle are governed by the UTT error in x and y. In Fig.'s 23 and 24, we summarize the effect of the UTT x and y errors on the astigmatism and coma curves respectively. The effect of the UTT error is to produce a bias in the centroid measurement in the direction of the UTT error. If this bias is in the direction of the laser launch telescope, the bias adds to the existing biases due to truncation, asymmetric elongation, quad-cell centroiding, causing a larger peak/valley in the astigmatism curves. If, however, the UTT error is in the opposite direction of the laser launch telescope, the bias subtracts from the existing biases and consequently the peak/valley of the astigmatism curve is reduced.
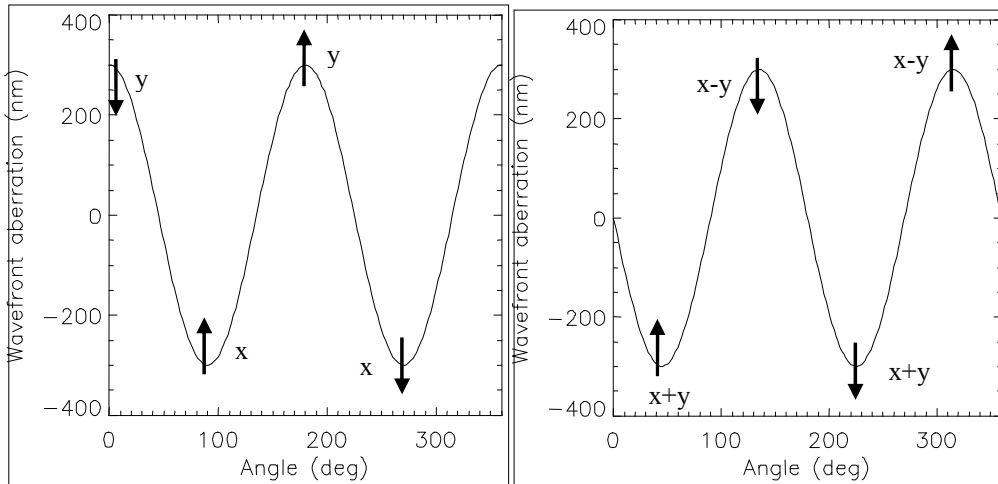
Figure 23 – The effect of an uplink tip-tilt error on the peaks and nulls of 0 degree astigmatism (left) and 45 degree astigmatism (right).
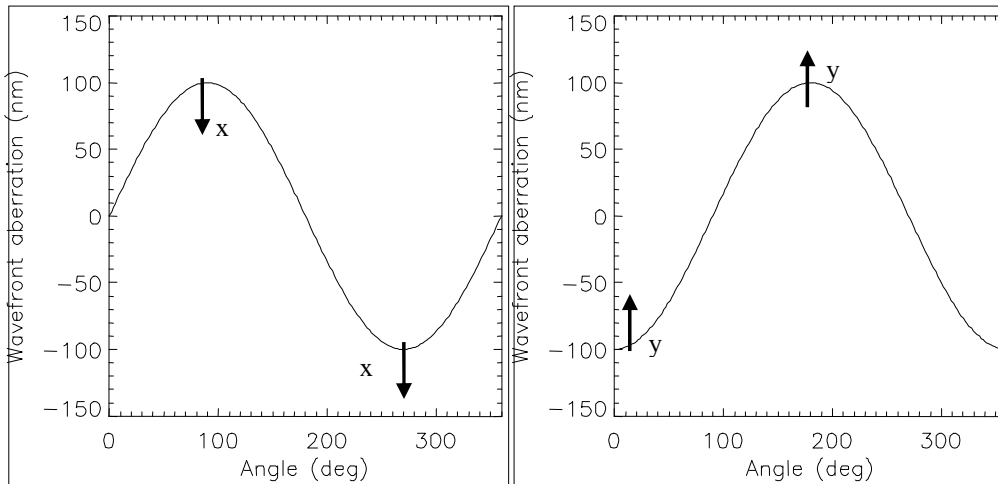
Figure 24 – The effect of an uplink tip-tilt error on the peaks and nulls of y coma (left) and x coma (right).

The uplink tip/tilt error has no noticeable effect on the spherical aberration. It is unclear what causes the spherical aberration observed on the telescope to be so much larger than that modeled here.

Using the relationships derived between the UTT x and y errors and the astigmatism and coma curves, we can say that the measured LGS aberrations of Section 1 exhibit an UTT error in the (+x,-y) direction. This is true for both nights, suggesting that the pupil-stop is de-centered. The error in the x direction is larger than that in the y direction.

3.4   Field stop

The size and shape of the field stop affects the truncation of the LGS spots and hence affects the LGS aberrations. In this subsection, we model a square field stop of linear dimension 4.2'' (twice the pixel scale) for the Keck II system, and compare with the circular field stop of Section 2. Because this square stop is the same dimension as the WFS FOV, the square stop is equivalent to no field stop at all. The LGS aberrations for the square field stop are plotted in Fig. 25. Comparing the aberrations for the square stop with those in Fig.'s 15 and 16 for a circular stop, we note that the 45 degree astigmatism term for the square stop is reduced to the same magnitude as the 0 degree term, and consequently the total aberration curve for the square stop is more-or-less constant. The coma and spherical aberration terms are of similar magnitude for the square and circular stops.
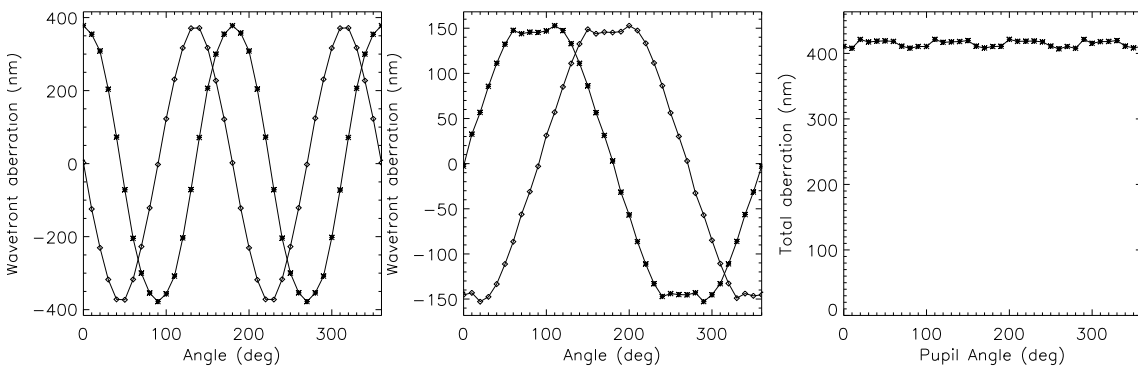

Figure 25 – The simulated magnitude of the LGS aberration modes as a function of pupil angle at zenith for a square field stop. Left: 0 degree astigmatism (*) and 45 degree astigmatism (◊); Center: y coma (*) and x coma (◊) ; Right: the total low order LGS.

3.5   LGS spot subdivision

The number of detector pixels used to sample the LGS images also affects the LGS aberrations. With a standard center-of-mass centroid operator, the more pixels there are, the higher the weighting on the portion of the spot farthest away from the center. This is shown in Fig. 26 for a quad-cell and 8x8 pixels with a spot of dimension 3 arc sec and total FOV of 4.2 arc sec.

When an asymmetric spot is truncated, the part of the spot that is truncated, and hence given a weighting of zero, would otherwise have the highest weighting on the centroid. To see this effect, we subdivide the LGS spots in a quad-cell (i.e. 2x2 pixels), with 4x4 pixels and 8x8 pixels, keeping the total FOV constant. The field stop is square and equal to the FOV. We consider two cases: 1) where there is some truncation of the spots using a 4.2'' FOV, and 2) where there is no significant truncation of the spots using a 8.4'' FOV.
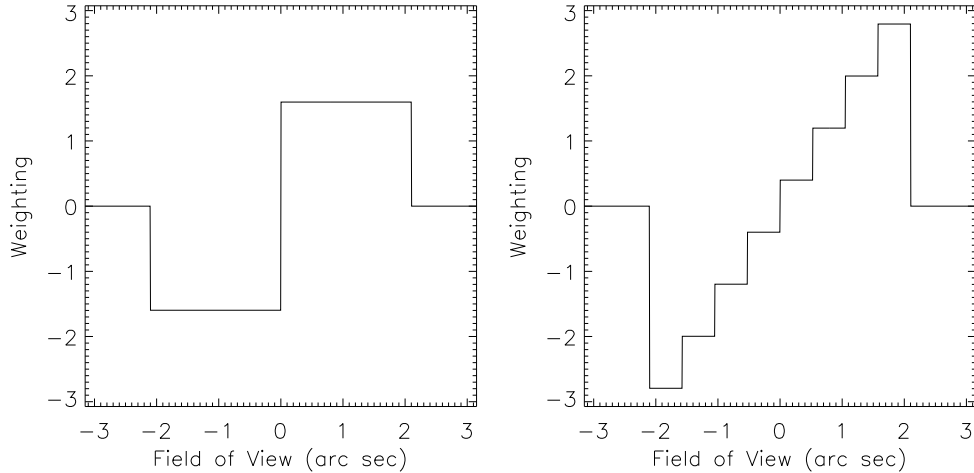
Figure 26 – The weighting over the FOV for a 3 arc sec spot with a center-of-mass centroid for (left) a quad-cell, and (right) 8x8 pixels.
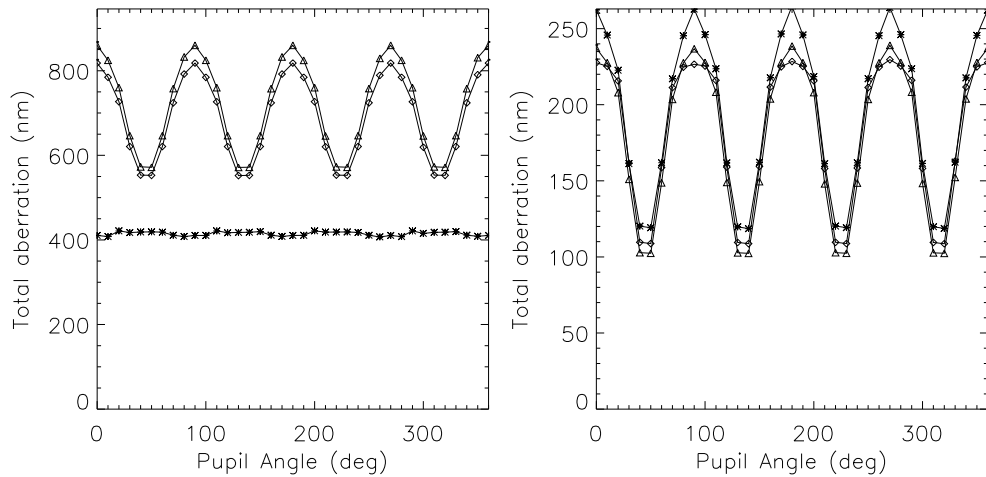
Figure 27 – Left: the total magnitude of the LGS low order aberrations for a FOV of 4.2 arc sec for 2x2 pixels (*), 4x4 pixels (◊), and 8x8 pixels (Δ). Right: the total magnitude of the LGS low order aberrations for a FOV of 8.4 arc sec for 2x2 pixels (*), 4x4 pixels (◊), and 8x8 pixels (Δ).

For the first case with a detector FOV of 4.2 arc sec, the total low-order LGS aberration is shown in Fig. 26. The LGS aberrations are lowest for 2x2 pixels, followed by 4x4 pixels and then 8x8 pixels. This is true for all pupil angles. The difference in going from a quad-cell to more pixels is greatest at 0, 90, 180 and 270 degrees because this is when the truncation is greatest, so the amplification of the truncation by the centroid operator is also the greatest.

For the second case, where we use a much larger FOV (8.4 arc sec) to avoid any significant truncation of the LGS spots, the total LGS aberrations are plotted in Fig. 27.

The total LGS aberration is largest for 2x2 pixels, with 4x4 and 8x8 pixels giving aberrations of approximately the same magnitude.

To summarize the simulation results presented in this subsection on the number of pixels used to subdivide the LGS spots, we see that if there is significant truncation of the spots, the aberrations are reduced by using a quad-cell. This is because the centroid operator weights the truncated portion of the spot more with more pixels, and so the bias due to truncation is increased with more pixels. In contrast, if there is no significant truncation of the spots, the LGS aberrations are reduced with more pixels, because the bias due to using a quad-cell centroid is reduced.

3.6   Field of view of the LGS WFS

The FOV of the LGS WFS affects the truncation of the LGS spots and hence the LGS aberrations. For the Keck II system, the FOV is equal to twice the plate scale of the quad-cell pixels. The total low order aberration as a function of the FOV for Keck II is shown in Fig. 28 for a pupil angle of 0 degrees. For a small FOV (i.e. 3 arc sec), there is significant truncation of the LGS spots and the LGS aberrations are large. As the FOV increases, the truncation is reduced and the LGS aberrations decrease. There is a local minimum at approximately 3.8'' where there is some truncation of the LGS spots, but the bias due to this truncation cancels to some extent the bias due to the quad-cell centroid of the asymmetric spots. As we increase the FOV further, although the truncation of the spots is decreasing, the LGS aberrations increase. At a FOV of 8 arc sec there is no truncation of the LGS spots and the LGS aberrations are at a minimum.
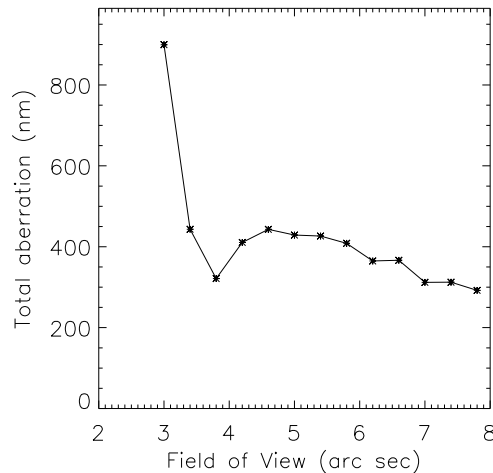

Figure 28 – The total LGS aberration as a function of the field of view (arc sec) for Keck II with a pupil angle of 0 degrees.

3.7   Seeing

The LGS aberrations are weakly dependent on the atmospheric seeing. The LGS images are convolved by the quadrature sum of the seeing (both up and down) and the charge diffusion of the pixels. In most cases, the charge diffusion (half the pixel scale) is significantly larger than twice the seeing, and so is the dominant term. Increasing the seeing can increase the truncation of the LGS images, increasing the bias due to truncation, but can also blur out the structure of the sodium layer, reducing another of the bias terms. As shown in Fig. 29, there is little dependence of the LGS WFS aberrations on the seeing over the expected range of seeing.
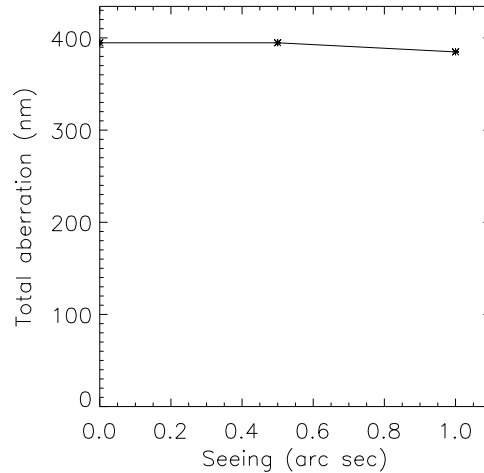

Figure 29 – The total LGS WFS aberration (nm) as a function of seeing (arc sec) for a 0 degree pupil angle for Keck II.

3.8   Correlation track algorithm

We compare using the correlation track algorithm [2] for determining the displacements of the LGS images, with the center-of-mass centroid algorithm used previously. The correlation track algorithm works by correlating the LGS image with a reference image for that subaperture. We have chosen to use the LGS images as the reference images, but with each reference image shifted such that the center-of-mass of the reference image is zero. The displacement of each subaperture is then found by shifting each subaperture image from its zero mean position to where the centroid from the correlation algorithm is zero.

Simulations using the correlation track and center-of-mass centroiding yielded LGS aberrations of exactly the same magnitude. The reason for this is that we are driving the centroid to zero, and the centroid will be zero when the LGS image is equal to the reference image. But the reference image has zero center-of-mass centroid, so the correlation track algorithm will give the same centroid as the center-of-mass centroid.

The correlation track method does improve the linearity of the wavefront sensor response, and consequently it is possible to drive the correlation centroid to zero more quickly than the center-of-mass centroid.

The same result will be true for the matched filter algorithm [3] for finding the subaperture displacements, because the reference images will still be truncated, and the true center unknown.

3.9   Temporal variation

On any night, the structure of the sodium layer is changing in time. In order to investigate the temporal nature of the LGS aberrations, we use a time series of 88 sodium profiles measured using the Colorado State LIDAR. These profiles have a temporal resolution of 72 seconds and a spatial resolution of 24m. The total LGS aberrations for the Keck II LGS AO system for a pupil angle of 0 degrees for these 88 sodium profile are plotted in Fig. 30 (left). The median total LGS aberration from this series of profiles is 76nm, which is significantly less than observed on the telescope. The difference in the LGS aberrations in the low order modes between consecutive time stamps is shown in Fig. 30 (right). The median difference in the LGS aberrations between consecutive frames is 20nm.
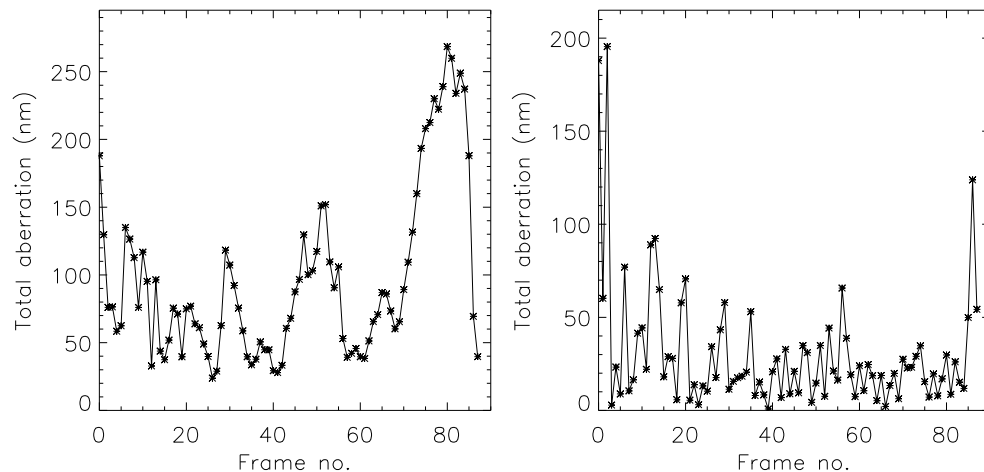
Figure 30 - Left: the total magnitude of the LGS low order aberrations (nm) for Keck II versus frame number of the LIDAR profile. The frames are sampled 72 seconds apart. Right: the difference in the LGS aberrations (nm) between consecutive frames.

4   Future Systems

In this section, we use our model developed to match the Keck II LGS aberrations to predict the LGS aberrations for future AO systems, Keck I NGWFC, Keck II NGWFC, Palomar and TMT.

4.1   Keck II NGWFC

The Keck II next generation wavefront controller (NGWFC) is side projected at a distance of 6.2m from the optical axis. There are two possible detectors to be used for the Keck II NGWFC: CCD-39 and CCID-56. There are two possible pixel configurations for the CCD-39: 2x2 pixels of dimension 3.0 arc sec, and 4x4 pixels of dimension 1.5 arc sec. In both cases, the field stops are square and of dimension 6.0 arc sec. For the CCID-56, there are 8x8 pixels of dimension 0.75 arc sec, and the field stop is 6.0 arc sec.

The LGS aberrations are plotted as a function of pupil angle in Fig. 31 for the CCD-39 2x2 pixels, Fig. 32 for the CCD-39 4x4 pixels, and Fig. 33 for the CCID-56. For the quad-cell case, the astigmatism, coma and total LGS aberrations are less than for the current Keck II system in the same conditions. This can be attributed to the increased pixel scale of the quad-cell pixels reducing the bias due to truncation. Comparing the three different pixel configurations, we note that the aberrations are smallest at all pupil angles for the quad-cell case. This is consistent with the results shown in Section 3.5, where it is shown the centroid operator amplifies the error due to truncation with more pixels. This error amplification is most noticeable in the 0 degree astigmatism and spherical aberration terms.
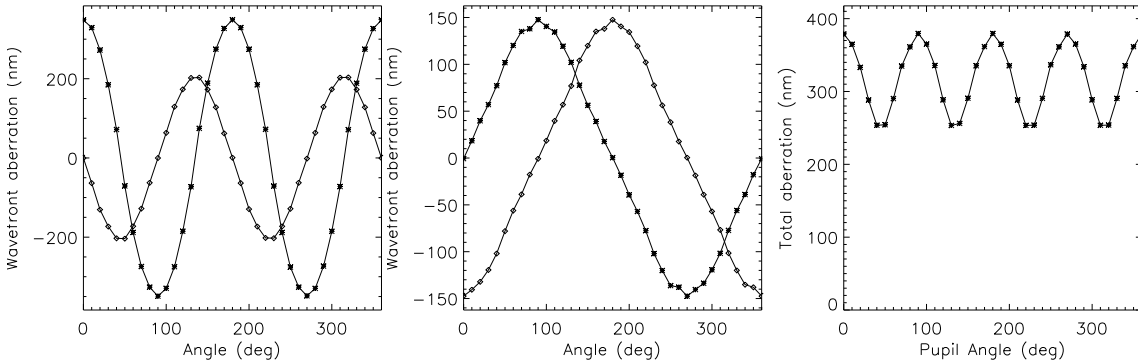

Figure 31 - The simulated magnitude of the LGS aberration modes as a function of pupil angle at zenith for the Keck II NGWFC CCD-39 with 2x2 pixels. Left: 0 degree astigmatism (*) and 45 degree astigmatism (◊);Center : y coma (*) and x coma(◊); Right: the total low order LGS aberration.
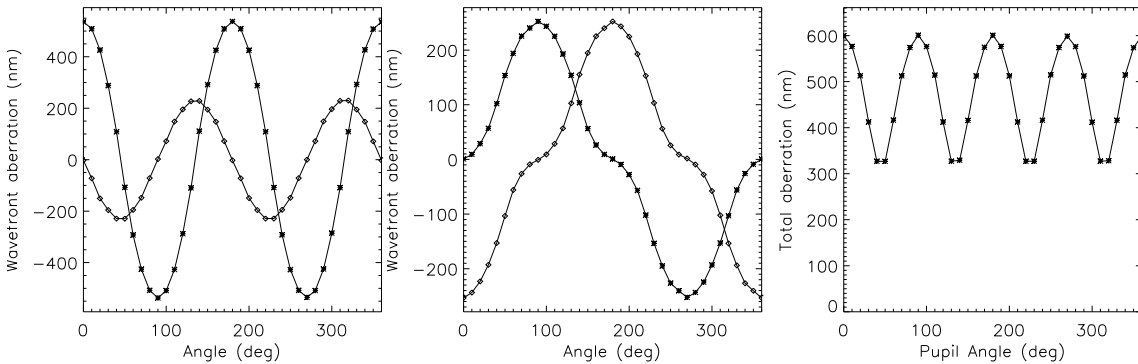
Figure 32 - The simulated magnitude of the LGS aberration modes as a function of pupil angle at zenith for the Keck II NGWFC CCD-39 with 4x4 pixels. Left: 0 degree astigmatism (*) and 45 degree astigmatism (◊);Center : y coma (*) and x coma(◊); Right: the total low order LGS aberration.

Figure 33 - The simulated magnitude of the LGS aberration modes as a function of pupil angle at zenith for the Keck II NGWFC CCID-56 with 8x8 pixels. Left: 0 degree astigmatism (*) and 45 degree astigmatism (◊); Center: y coma (*) and x coma (◊); Right: The total low order LGS aberration.
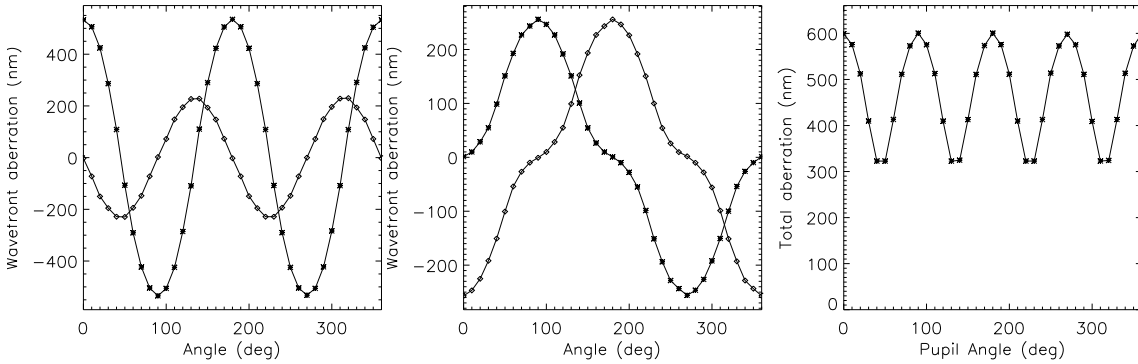
4.2   Keck I NGWFC

Keck I will propagate the laser from behind the center of the secondary. Again, there are two possible detectors: CCD-39 and CCID-56. For the CCD-39, the pixel configurations are either 2x2 pixels of dimension 2.4 arc sec, or 4x4 pixels of 1.2 arc sec. For the CCID-56 pixel configuration, there are 8x8 pixels of dimension 0.75 arc sec. In all cases, there is a square field stop of 4.8 arc sec a side. Because the laser is projected from behind the secondary, there is no dependence of the aberrations on pupil angle, and instead we tabulate the LGS aberrations in Table 1. Most of the low order Zernikes are zero, so we only tabulate any of the first 30 terms that are non-zero. The phase screen represented by the sum of the low order aberrations is plotted in Fig. 34.
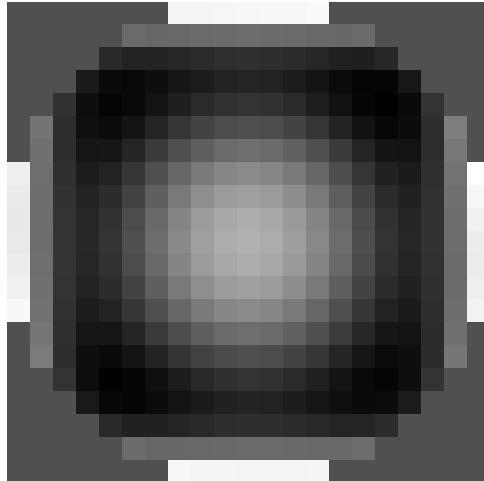
Figure 34 – The total low order LGS aberration for the centrally projected K1 NGWFC with 2x2 pixels.

Fig. 34 shows that the LGS aberrations are circularly symmetric at the center of the pupil, but square symmetric at the edges of the pupil. The circular symmetry arises from the central projection of the laser, and the square symmetry from the square field stop (square extent of the pupils). As shown in Table 1, the only non-zero terms of the first 30 Zernikes for the K1 NGWFC are Z11 and Z22 (circularly symmetric), and Z14 and Z26 (square symmetric). The proposed pixel configurations make little difference to the magnitude of the LGS aberrations. If the field stop were circular instead of square, the square symmetric (Z14 and Z26) terms are near zero, showing these terms arise due to the square field stop. However, the circular field stop leads to a higher spherical aberration term (49 nm), such that the total aberration is greater with a circular stop than a square stop.

	Wavefront aberration (nm)		
Zernike Mode	CCD-39 2x2	CCD-39 4x4	CCID-56 8x8
Z11 (Spherical)	39	38	34
Z14	26	28	25
Z22 (5th order spherical)	-1	3	4
Z26	1	7	7
Total	47	48	43

Table 1 – LGS aberrations by Zernike mode for the Keck I NGWFC

4.3   Palomar

The 5.1m Hale telescope at Mt. Palomar has a centrally projected laser. The LGS WFS is a Shack-Hartmann with 16x16 subapertures. Each subaperture has a quad-cell detector with pixels of dimension 1.2 arc sec for a FOV of 2.4 arc sec. There are 174 active subapertures. The total low order LGS aberration expected for Palomar is 5 nm. The only non-zero mode of the first 30 Zernikes is spherical aberration which is 5 nm. For Palomar, the LGS aberrations are insignificant, which is due to the central projection of the laser and small aperture size.

4.4   Lick

Like Keck II, the Lick laser is side projected. The Lick primary mirror is 3m in diameter. The LGS WFS is an 8x8 lenslet array, with the central 4 lenslets obscured by the secondary. The WFS detector consists of quad-cells.

I need the laser offset (1.5m+?), and plate scale of the pixels to run the simulations for Lick.

4.5   TMT

The Thirty Meter Telescope (TMT) has a 30 meter diameter primary and will project the laser from the center of the secondary. In order to overcome the cone effect, TMT intends to use an asterism of six LGS: one on-axis, and the other five equally spaced on a ring of radius 35 arc sec. Because the LGS are so closely spaced (the difference in zenith angle between any two LGS is << 1 deg), each LGS will experience approximately the same LGS aberrations, and so we consider here the on-axis LGS only. The proposed LGS WFS(s) are Shack-Hartmann WFS of the order 60x60 subapertures. TMT will employ the radial format CCD, with 16x4 pixels per subaperture of dimension 0.5''. Here we assume a detector of 16x16 pixels of 0.5'' to bound the problem. We also assume a square field stop of dimensions 8.0x8.0 arc sec, center-of-mass centroiding, and that all the subapertures within the extent of the primary mirror are active at any one time.

	Wavefront aberration (nm)	
Zernike Mode	Gaussian profile	Sum of 2 Gaussians profile
Z11 (Spherical)	260	834
Z14	100	338
Z22 (5th order spherical)	-8	42
Z26	29	158
Total	281	915

Table 2 – LGS aberrations by Zernike mode for TMT

The non-zero magnitude LGS aberrations modes for TMT are displayed in Table 2. As for the centrally projected K1 NGWFC, spherical aberration is the largest term, followed by Z26, Z14 and Z22. These four Zernike terms are significantly larger for TMT than for

the Keck I NGWFC which is due to the much larger telescope diameter for TMT, meaning that the subapertures furthest away from the center are more elongated.

5   Conclusions

In this report, we have successfully modeled the LGS aberrations observed at WM Keck Observatory, and have used this model to characterize the parameter space that affects the LGS aberrations, and also to predict the LGS aberrations of future LGS AO systems. In particular, we note that the LGS aberrations are a strong function of sodium structure, and this explains the significant difference in magnitude of the LGS aberrations between nights. The LGS aberrations can be significantly reduced by projecting the laser from behind the secondary mirror of the telescope, and by increasing the FOV of the wavefront sensor detector. With regard to future systems, the LGS aberrations increase exponentially with increasing telescope diameter.

6   References

[1] MA van Dam, AH Bouchez, D Le Mignant, and P. Wizinowich, "Quasi-static aberrations induced by laser guide stars in adaptive optics," Opt. Exp. 14, 7535-7540 (2006).

[2] L.A. Poyneer, "Scene-based Shack-Hartmann wave-front sensing: analysis and simulation," Applied Optics 42, 5807-5815 (2003).

[3] L. Gilles and B.L. Ellerbroek, "Shack-Hartmann wavefront sensing with elongated sodium laser beacons: centroiding versus matched filtering," Applied Optics 45, 6568-6576 (2006).